



Missouri University of Science and Technology  
Scholars' Mine

---

Electrical and Computer Engineering Faculty  
Research & Creative Works

Electrical and Computer Engineering

---

01 Oct 2008

## Prediction of Effective Permittivity of Diphasic Dielectrics Using an Equivalent Capacitance Model


Sandeep K. Patil

Marina Koledintseva  
*Missouri University of Science and Technology*

Robert W. Schwartz  
*Missouri University of Science and Technology*

Wayne Huebner  
*Missouri University of Science and Technology, huebner@mst.edu*

Follow this and additional works at: [https://scholarsmine.mst.edu/ele\\_comeng\\_facwork](https://scholarsmine.mst.edu/ele_comeng_facwork)

 Part of the [Electrical and Computer Engineering Commons](#), and the [Materials Science and Engineering Commons](#)

---

### Recommended Citation

S. K. Patil et al., "Prediction of Effective Permittivity of Diphasic Dielectrics Using an Equivalent Capacitance Model," *Journal of Applied Physics*, American Institute of Physics (AIP), Oct 2008. The definitive version is available at <https://doi.org/10.1063/1.2976173>

This Article - Journal is brought to you for free and open access by Scholars' Mine. It has been accepted for inclusion in Electrical and Computer Engineering Faculty Research & Creative Works by an authorized administrator of Scholars' Mine. This work is protected by U. S. Copyright Law. Unauthorized use including reproduction for redistribution requires the permission of the copyright holder. For more information, please contact [scholarsmine@mst.edu](mailto:scholarsmine@mst.edu).

# Prediction of effective permittivity of diphasic dielectrics using an equivalent capacitance model

S. K. Patil,<sup>1,a)</sup> M. Y. Koledintseva,<sup>2</sup> R. W. Schwartz,<sup>1</sup> and W. Huebner<sup>1</sup>

<sup>1</sup>*Department of Materials Science and Engineering, Missouri University of Science and Technology, Rolla, Missouri 65409, USA*

<sup>2</sup>*Department of Electrical and Computer Engineering, Missouri University of Science and Technology, Rolla, Missouri 65409, USA*

(Received 20 May 2008; accepted 1 July 2008; published online 7 October 2008)

An analytical model based on an equivalent capacitance circuit for expressing a static effective permittivity of a composite dielectric with complex-shaped inclusions is presented. The dielectric constant of 0–3 composites is investigated using this model. The geometry of the capacitor containing a composite dielectric is discretized into partial parallel-plate capacitor elements, and the effective permittivity of the composite is obtained from the equivalent capacitance of the structure. First, an individual cell diphasic dielectric (a high-permittivity spherical inclusion enclosed in a lower permittivity parallelepiped) is considered. The capacitance of this cell is modeled as a function of an inclusion radius/volume fraction. The proposed approach is extended over a periodic three-dimensional structure comprised of multiple individual cells. The results of modeling are compared with results obtained using different effective medium theories, including Maxwell Garnett, logarithmic, Bruggeman, series, and parallel mixing rules. It is found that the model predictions are in good agreement with the experimental data. The equivalent capacitance model may be applied to composites containing inclusions of any geometry and size. Although the method presented is at static electric field, it can be easily generalized for prediction of frequency-dependent effective permittivity. © 2008 American Institute of Physics. [DOI: [10.1063/1.2976173](https://doi.org/10.1063/1.2976173)]

## I. INTRODUCTION

The effective properties of dielectric mixtures have been investigated for more than 100 years, with the earliest known reference for prediction of effective dielectric constant of a mixture being attributed to Poisson.<sup>1</sup> Rayleigh calculated the effective permittivity of a mixture based on spherical or cylindrical inclusions in a rectangular lattice, and his results provided a connection between the properties of the mixture and the properties of the inclusions and macroscopic medium.<sup>2</sup> One of the classical and most widely used formulations to calculate effective permittivity of dilute mixtures is the Maxwell Garnett (MG) theory,<sup>3–6</sup> which was first formulated for spherical inclusions.

The Maxwell Garnett theory was also extended for ellipsoidal inclusions (spheroids, cylinders, and disks).<sup>3</sup> The theory is also applicable for inclusions of any arbitrary ellipsoidal shape (spheroids, cylinders, and disks) through introduction of depolarization factors.<sup>6,7</sup> However, an arbitrary inclusion shape cannot be accurately accounted for, other than by approximation by the closest ellipsoidal shape.<sup>8</sup>

There have been numerous other models developed to predict the effective permittivity of composites. To account for nonellipsoidal shapes, Weiner<sup>9</sup> proposed form factors for inclusions with cylindrical and lamellar shapes. Rushman and Striven<sup>10</sup> used these form factors to explain the impact of porosity upon the dielectric constant of barium titanate (BT).

Experimental evidence for the Weiner<sup>9</sup> mixing rule and its applicability to porous dielectrics was confirmed by Kingery<sup>11</sup> in 1960.

Bruggeman's<sup>12</sup> effective medium theory (EMT) is better suited for denser composites than the MG rule. However, EMT does not allow for correlation between the inclusions, i.e., it assumes that each inclusion is surrounded by the same effective medium.<sup>13</sup>

The empirically derived logarithmic mixing rule is also used for description of effective properties of composites.<sup>14</sup> In many cases it appears to fit experimental data; however in some cases it may be fortuitous, as pointed out by Payne.<sup>15</sup>

This paper is focused on the development of a simple analytical model to predict the effective permittivity of a dielectric composite that is valid for any volume fraction of inclusions, and can be applied to inclusions of any shape. The model presented herein is based on the discretization of a dielectric body of any shape into simple parallel-plate partial capacitor elements. By using this approach, actual inclusion shapes can be accounted for. The effective permittivity is then calculated based on the capacitance of the appropriate equivalent circuit.

The specific example of this approach presented in this paper is a geometrically isotropic (spherical) inclusion of higher permittivity in a host dielectric of lower permittivity. The host dielectric is a parallelepiped, in particular, a cube. This structure is called "an individual cell" (or just "a cell"). The capacitance of a cell is modeled as a function of the radius or volume fraction of the inclusion. The approach is subsequently extended over a periodic three-dimensional (3D) structure with multiple individual cells. This is analo-

<sup>a)</sup>Electronic mail: [patil.sandeep7@gmail.com](mailto:patil.sandeep7@gmail.com).

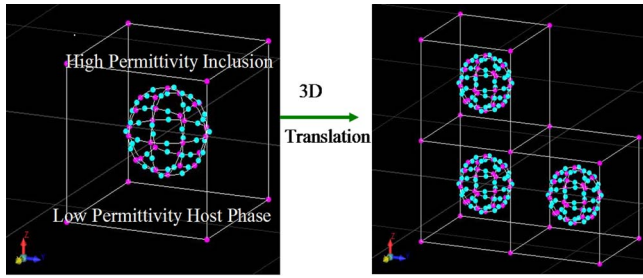


FIG. 1. (Color online) Basic building block of a composite sphere enclosed in a cube and its 3D translation in the  $x$ ,  $y$ , and  $z$  directions.

gous to the extensively studied epoxy/BaTiO<sub>3</sub> systems, for which substantial experimental data are available.<sup>16–22</sup> Recently, 0–3 high-permittivity polymer-based composites have been increasingly investigated for both comparatively low-energy embedded capacitor technology<sup>16–21</sup> and high-energy density applications for pulsed power capacitors.<sup>22</sup>

Results of the equivalent capacitance approach that is developed here are compared with computations based on the MG mixing theory, Bruggeman’s<sup>12</sup> mixing rule, logarithmic mixing rule, and recently reported experimental results. The mathematical formulation for the equivalent capacitance model is presented below in Sec. II, results for the model are demonstrated in Sec. III with comparison to the MG model, and conclusions regarding the utility of the model are presented in Sec. IV.

**II. MATHEMATICAL FORMULATION**

**A. One individual capacitor cell**

A general diphasic slab with a 3D periodic structure of inclusions is subdivided into individual cells (cubes), each containing one inclusion of a higher permittivity surrounded by a host material of a lower permittivity. Figure 1 shows the basic building block of the composite and its 3D translation. The structure that is modeled as an ordered composite.

First, consider an individual cell with a sphere placed at the center of the cube. The inclusion size is varied from 0.1 to 0.54  $\mu\text{m}$  within a host phase cube with dimension of 1.1  $\mu\text{m}$ . In the present model, it is assumed that both the inclusion and host are linear isotropic and homogeneous dielectric materials.

A homogeneous static electric field is applied along the vertical dimension of the cell. Then, any cell is an individual capacitor with inhomogeneous contents, and it can be discretized into parallel and series parallel-plate partial capacitors with capacitances given by

$$C_p = \frac{\epsilon_0 \epsilon_p A_p}{d_p}, \tag{1}$$

where  $\epsilon_0 = 8.854 \times 10^{-12}$  F/m is the vacuum permittivity,  $\epsilon_p$  is the relative permittivity of a dielectric in a partial capacitor,  $A_p$  is an area of the partial capacitor plates, and  $d_p$  is the thickness of the partial capacitor. The resultant capacitance of a whole cell can be calculated using an appropriate equivalent circuit model.

Figure 2 shows how the discretization process is implemented for a basic cubic building block with a spherical

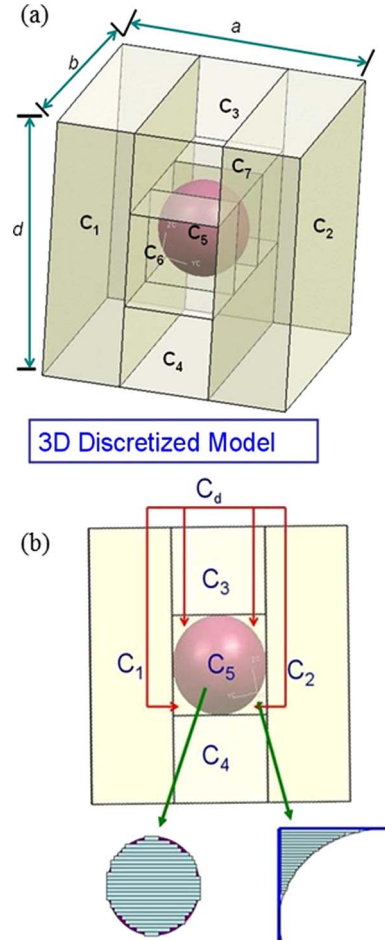


FIG. 2. (Color online) 3D view of discretized diphasic dielectric body and 2D planar view of discretized diphasic dielectric body showing discretization pathway for corner shape and inclusion sphere.

inclusion. This figure also shows a planar projection of the 3D view. The individual cell is divided into partial capacitors (numbered 1–7), and the corner capacitors around the sphere labeled as  $C_d$ . An equivalent circuit for this structure is shown in Fig. 3. Below, the explicit formulas for calculating these partial capacitances are given.  $C_1$  and  $C_2$  are the capacitances on the left and the right sides of the inclusion. If the structure is symmetrical,  $C_1$  and  $C_2$  are identical and

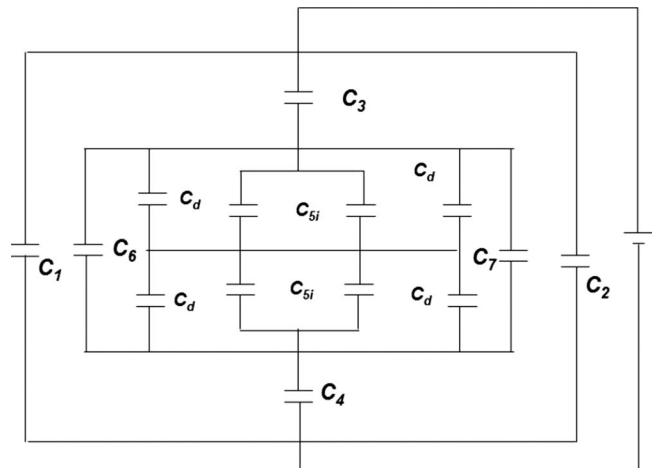


FIG. 3. Diphasic dielectric represented by an equivalent circuit.

linearly decrease as the radius of the inclusion increases. These capacitances may be calculated according to

$$C_1 = C_2 = \frac{\epsilon_0 \epsilon_h (a_c/2 - r) b_c}{d_c}, \quad (2)$$

where  $\epsilon_h$  is the relative permittivity of the host material,  $a_c$ ,  $b_c$ , and  $d_c$  are the length, width, and height of the individual cell (for the particular case of a cube,  $a_c = b_c = d_c$ ), and  $r$  is the radius of the inclusion. The partial capacitances  $C_3$  and  $C_4$  are associated with the elements located on the top and the bottom of the inclusion, and their values are calculated as

$$C_3 = C_4 = \frac{2\epsilon_0 \epsilon_h (2b_c r)}{d_c - 2r}. \quad (3)$$

The partial capacitors  $C_6$  and  $C_7$  are not seen in this planar view—they are located in front and behind the sphere, but can be seen in a 3D view (Fig. 2). Their values are calculated as

$$C_6 = C_7 = \frac{\epsilon_0 \epsilon_h (b_c - 2r)}{2}. \quad (4)$$

Figure 2 also shows the discretization approach utilized for the corner shape and inclusion sphere. The capacitance of the corner capacitor elements is calculated using elemental slices parallel to the cell's electrode planes.

These partial capacitors are connected in series, and the integration over the space of the corners is then used to evaluate the total capacitance of these volumes (see the derivation in Appendix A). The total capacitance for all four corner elements—two bottom and two top ( $i=1, \dots, 4$ )—is

$$C_d = \frac{\epsilon_0 \epsilon_h r \pi}{2} \frac{1}{\frac{1}{\sqrt{\frac{4}{\pi} - 1}} \arctan \left[ \frac{1}{\sqrt{\frac{4}{\pi} - 1}} \right]}. \quad (5)$$

To calculate the capacitance of the high-permittivity sphere, it is convenient to cut it into thin parallel slices and consider the series connection of these elements, corresponding to the slices. As shown in Appendix B, the integration procedure yields the capacitance of the quarters of the dielectric sphere  $C_{5_i}$  ( $i=1, \dots, 4$ ), which is the same as for the total sphere,

$$C_5 = C_{5_i} = \frac{\epsilon_0 \epsilon_i \pi r}{2 \int_0^{\pi/2} \frac{d\theta}{\cos(\theta)}}. \quad (6)$$

To assure convergence of the integral in the denominator, zero in the integration was substituted by  $10^{-7}$ . Since the capacitor elements  $C_5$ ,  $C_6$ ,  $C_7$ , and  $C_d$  are all in parallel (see Fig. 2), and they are in series with  $C_3$  and  $C_4$ , the equivalent capacitance for the central region of the cube is

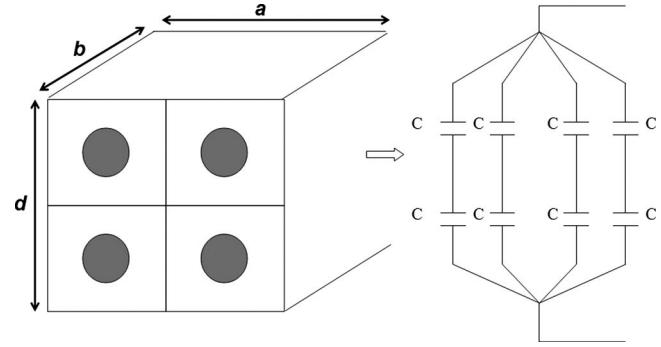


FIG. 4. Discretization pathway for  $N^3$  capacitor cells.

$$C_{eq1} = \frac{1}{\frac{1}{C_3} + \frac{1}{C_4} + \frac{1}{C_5 + C_6 + C_7 + C_d}}. \quad (7)$$

This capacitance  $C_{eq1}$ , as shown in Fig. 2, in its turn, is parallel with the left and right capacitors  $C_1$  and  $C_2$ , and therefore, the total equivalent capacitance is

$$C_{cell} = C_1 + C_2 + C_{eq1}. \quad (8)$$

Then, assuming that a homogeneous dielectric fills the space between the cell capacitor plates, the effective permittivity can be calculated from the expression for total capacitance  $C_{cell}$  of the cell as

$$\epsilon'_{eff} = \frac{C_{cell} d_c}{\epsilon_0 a_c b_c}. \quad (9)$$

The effective permittivity ( $\epsilon'_{eff}$ ) captures the shape of the inclusion, and there are no restrictions on the inclusion size. In general, the shape of an inclusion can be arbitrary, although different integration schemes are required. For example, ellipsoidal, tetrahedral, and other straight-line geometries would be relatively straightforward, while arbitrary curvilinear shapes would require special discretization schemes.

## B. $N^3$ individual capacitor cells

The equivalent capacitance model may be extended for the case of multiple inclusions. Consider a case when there are  $N$  inclusions in the form of spheres along any of three dimensions of the total capacitor. This means that there are  $N^3$  elemental capacitor cells in the structure under consideration. The capacitor cells in vertical branches are connected in series, while all the branches are connected in parallel, as shown in Fig. 4. The capacitance in any branch is

$$C_{branch} = \frac{C_{cell}}{N}. \quad (10)$$

Because there are  $N^2$  vertical branches, the total capacitance is

$$C_{\Sigma} = \frac{C_{cell}}{N} N^2 = N C_{cell}. \quad (11)$$

where the capacitance  $C_{cell}$  is calculated as in Sec. II A. If the dimensions of the total capacitor are  $a$ ,  $b$ , and  $d$ , then the

dimensions of an individual cell are, respectively,

$$\begin{aligned} a_c &= a/N, \\ b_c &= b/N, \\ d_c &= d/N. \end{aligned} \quad (12)$$

Then, the effective permittivity of an inhomogeneous dielectric inside the total capacitor can be calculated as

$$\epsilon'_{\text{eff}} = \frac{C_{\Sigma} d}{ab\epsilon_0}. \quad (13)$$

The effective permittivity of an inhomogeneous dielectric obtained using this method may be compared with the MG mixing rule results. The simplest formulation is for a mixture of a host material with relative permittivity  $\epsilon_h$  and spherical inclusions with relative permittivity  $\epsilon_s$ , as given by<sup>3,4,9</sup>

$$\epsilon_{\text{eff MG}} \cong \epsilon_h + \frac{3f_s \epsilon_h (\epsilon_s - \epsilon_h) / (\epsilon_s + 2\epsilon_h)}{1 - f_s (\epsilon_s - \epsilon_h) / (\epsilon_s + 2\epsilon_h)}, \quad (14)$$

where  $f_s = V_s / V_{\Sigma}$  is the volume fraction of spherical inclusions in the total mixture and  $V_s$  is the volume of inclusion and  $V_{\Sigma}$  is the total volume of the composite.

It is also informative to compare the equivalent capacitance model with the formula for the logarithmic mixing rule, given by

$$\epsilon_{\text{eff logarithmic}} \cong V_h \log \epsilon_h + V_i \log \epsilon_i, \quad (15)$$

and to the formula for the Bruggeman<sup>12</sup> mixing rule, given by

$$\frac{\epsilon_i - \epsilon'_{\text{eff}}}{\epsilon_i - \epsilon_h} = \frac{1 - V_i}{\sqrt[3]{\epsilon_h / \epsilon_{\text{eff}}}}. \quad (16)$$

Here,  $V_h$  and  $\epsilon_h$  are the volume fraction and permittivity of the host phase, and  $V_i$  and  $\epsilon_i$  are the volume fraction and permittivity of the inclusion phase, respectively.

### III. RESULTS AND DISCUSSION

The first calculation is for the capacitance of a cube containing one spherical inclusion placed in the center of the cube. The inclusion is a high-permittivity dielectric, for example, BT, with relative permittivity assumed to be  $\epsilon_i = 1900$ . The cube surrounding the BT sphere is a low-permittivity phase, for example, with relative permittivity  $\epsilon_h = 4$  (polyamides, epoxy, etc). The cube has the following dimension:  $a_c = b_c = d_c = 1.1 \mu\text{m}$ . This size is chosen to imitate a real structure of a polymer ceramic dielectric. The radius of the sphere is varied, and, the volume fraction of the inclusion is also varied. For this capacitor structure, the maximum inclusion volume fraction is approximately 52.3%. The electric field is applied in the vertical direction, as dictated by the equivalent capacitance model outlined above. The capacitance of this structure is calculated according to the formulas presented in Sec. II A. The analytical software MAPLE 10 was used to carry out the computations presented below.

$C_1$ - $C_2$  : The capacitance of elements  $C_1$  and  $C_2$  are equal

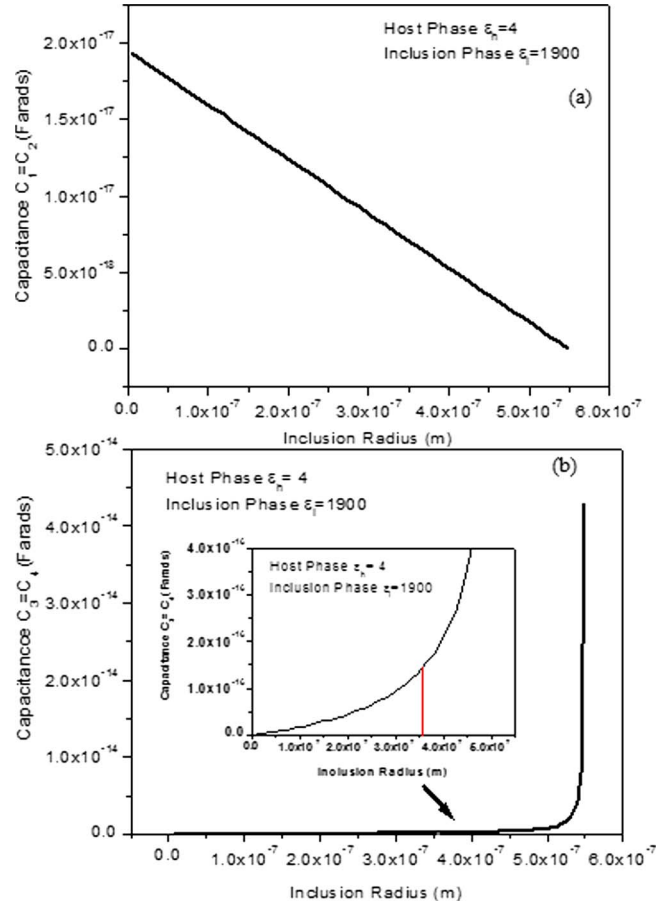


FIG. 5. (Color online) Magnitude of capacitances of capacitor elements  $C_1$ ,  $C_2$ ,  $C_3$ , and  $C_4$  as a function of inclusion radius ( $r$ ).

since both capacitors have the same low permittivity  $\epsilon_h$ , the same area, and the same thickness. The capacitance data for both capacitors  $C_1$  and  $C_2$  as a function of the radius of the inclusion is plotted in Fig. 5(a). Capacitances  $C_1$  and  $C_2$  show a linear decrease as the inclusion radius increases. This is an expected result since with increasing inclusion radius, there is a linear decrease in the area of the capacitor plates, while its thickness remains constant.

$C_3$ - $C_4$  : The capacitances of capacitors  $C_3$  and  $C_4$  are also equal. These partial capacitors located on top and bottom of the spherical inclusion have the same area and thickness. The capacitance data for both capacitors  $C_3$  and  $C_4$  as a function of radius of the inclusion is plotted in Fig. 5(b). It is seen that when the inclusion radius is small ( $r \leq 0.2 \mu\text{m}$ ), there is a minimal increase in capacitance [ $(0.01 - 0.1) \times 10^{-14}$  F]. This is because the area of the capacitor “plates” remains small (area  $< 0.4 \mu\text{m}^2$ ), while the thickness of the dielectric remains relatively high ( $d \geq 0.6 \mu\text{m}$ ).

After the radius becomes approximately  $\frac{1}{3}$  of the cell dimension, the area of the capacitor increases, the thickness concurrently decreases, and there is a rapid increase in capacitance as  $\propto r^3$ . It is observed that beyond the inclusion radius of  $0.53 \mu\text{m}$ , there is a rapid increase in the capacitances of  $C_3$  and  $C_4$ . When inclusions start touching the top and bottom of the host phase cube, the corresponding capacitances go to infinity. In computations, it is assumed that the thickness of the dielectric layers for  $C_3$  and  $C_4$  is at least 1%

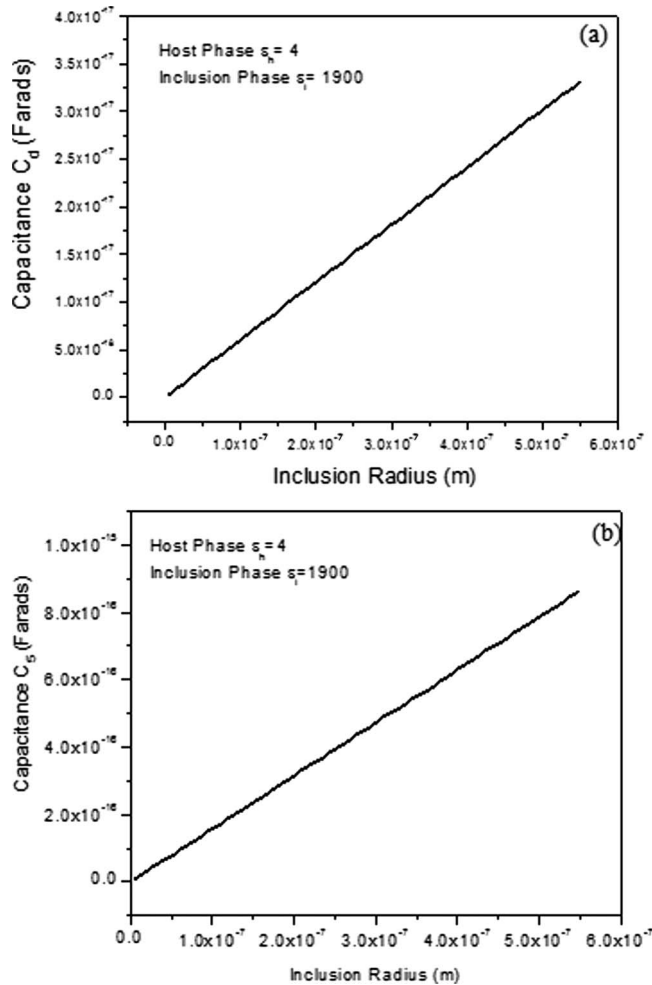


FIG. 6. Magnitude of capacitances of capacitor elements  $C_d$  and  $C_5$  as a function of inclusion radius ( $r$ ).

of the inclusion radius. Therefore, this model is applicable until the inclusion radii are about  $0.5445 \mu\text{m}$ .

$C_d$ : The capacitance of the corner elements depend on the shape of the inclusion. There is a linear increase in this capacitance with inclusion radius, as shown in Fig. 6(a). This capacitance  $C_d$  becomes significant when the radius of the inclusion increases.

$C_5$ : The capacitor  $C_5$  is constituted of the high-permittivity phase. The capacitance data for capacitor  $C_5$  as a function of inclusion radius are plotted in Fig. 6(b). There is a linear increase in  $C_5$  as the radius of the inclusion increases, which is an expected result.

$C_6$ - $C_7$ : The capacitances  $C_6$  and  $C_7$  located in front and back of the inclusion show a linear decrease in the capacitance with increasing inclusion radius, similar to the behavior of  $C_1$  and  $C_2$ .

Figure 7(a) shows that capacitance  $C_6$  (and  $C_7$  as well) decreases as a function of inclusion radius. This is because the area of the corresponding capacitor plates decreases linearly as the inclusion radius increases.

$C_\Sigma$ : The total equivalent capacitance for the diphasic composite as a function of inclusion radius is plotted in Fig. 7(b), and it shows a trend similar to that for the partial capacitances  $C_3$  and  $C_4$  since at larger inclusion radii ( $r$

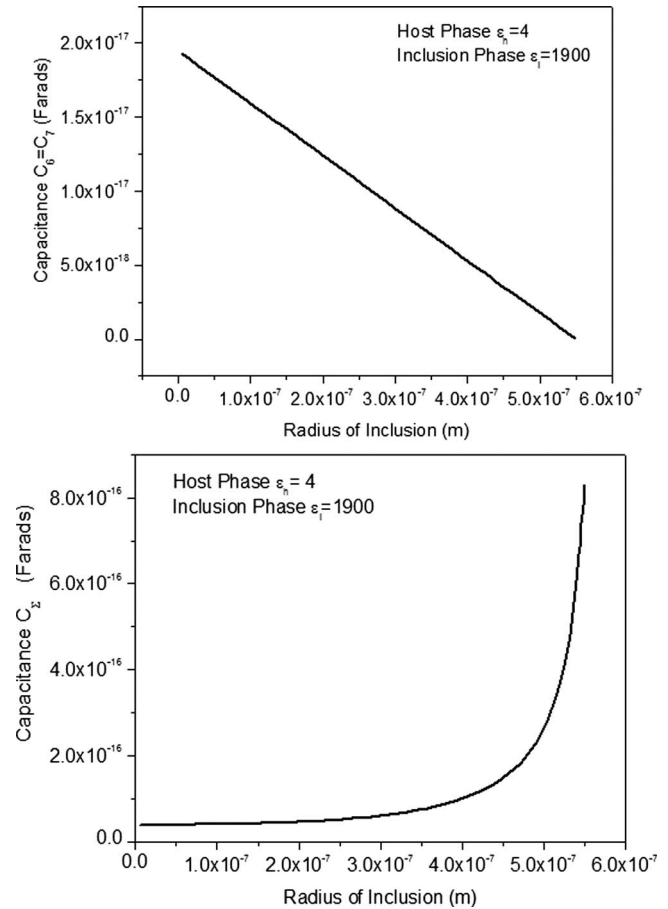


FIG. 7. Magnitude of capacitances of capacitor elements  $C_6$ ,  $C_7$ , and  $C_\Sigma$  as a function of inclusion radius ( $r$ ).

$\geq 0.4 \mu\text{m}$ ) these two capacitances dominate.

The effective permittivity of the composite, calculated through the total capacitance, is illustrated in Fig. 8. According to the equivalent capacitance model, the predicted effective permittivity for the inclusion volume fraction range of

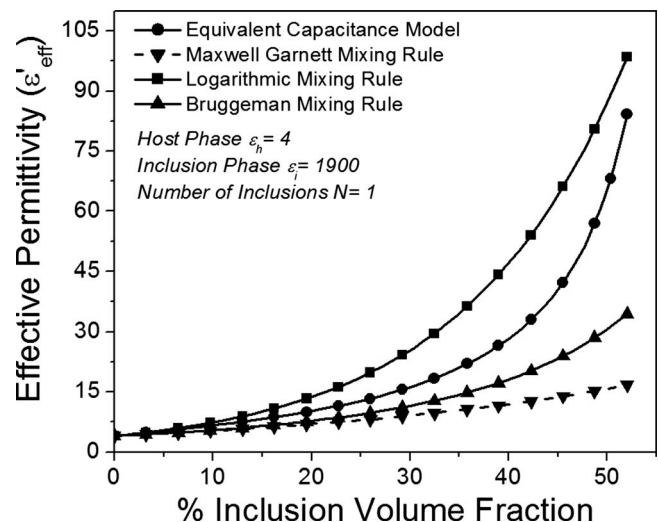


FIG. 8. Effective permittivity of composite predicted by equivalent capacitance model as a function of inclusion volume fraction for  $N=1$  inclusions and its comparison to predictions of the MG mixing theory, the Bruggeman (Ref. 12) mixing rule, and logarithmic mixing rule.

0%–35% increases from 4 to 15. The predicted permittivity for inclusion volume fraction variation from 35% to 52% increases from 15 to 80. When the radius of the spherical inclusions reaches approximately  $\frac{1}{3}$  of the cell dimension, the rate of the effective permittivity increase becomes greater. The calculated maximum permittivity is around 80 for the volume fraction of approximately 52% and the dielectric contrast (*ratio of permittivity of inclusion phase to permittivity of host*) of 300.

Figure 8 also shows the effective permittivity as a function of inclusion radius for the same composite calculated using the MG mixing rule, logarithmic rule, and Bruggeman<sup>12</sup> formulation. The trend shown by the equivalent circuit capacitance model is similar to that for the other mixing rules. However the slope of the dependence equivalent capacitor model becomes steeper as the inclusion radius approaches its limiting point ( $r > 0.54 \mu\text{m}$ ). The equivalent capacitance model results lie between the logarithmic rule, which overestimates the effective permittivity, and the Bruggeman model predictions.

The equivalent capacitance model was also tested for multiple inclusions as opposed the single inclusion case reported above. A composite system with the same host cube dimensions but with 1000 high-permittivity inclusions is considered. The total capacitor dimensions are the same as in the previous example with one spherical BT inclusion in host ( $a=b=d=1.1 \mu\text{m}$ ). In the equivalent capacitance model, the total structure contains 1000 individual cells.

The maximum radius of each inclusion is ten times smaller than that in the previous single cell example. In this particular case, the inclusion size is reduced, and it varies from 10 nm to a maximum of 54 nm, as opposed to the earlier case when the single inclusion size varied from 0.1 to  $0.54 \mu\text{m}$ . This structure is an ordered nanoscale composite. It has been verified that the predictions of the equivalent capacitance model for the multiple inclusion case remain identical to the single inclusion case. The model suggests consistent results for analogous volume fraction, no matter how many inclusions of the same shape are present. The results are independent of inclusion size, but they capture inclusion shape.

In a parallelepiped with a homogeneous static electric field applied along one of its dimensions, there is a continuous linear variation of the electrostatic potential along this direction.<sup>23</sup> That is why cutting the structure into parallel-plane slices and applying rules for calculating equivalent series and parallel capacitances allows for taking into account electric field present within this slices. The model satisfies all boundary conditions for electric field and potential between the partial capacitor elements. The accuracy of these computations depends on how fine the discretization is, and the discretization is defined by the shape of inclusions.

The equivalent capacitance model is validated by comparison with experimental data for two different diphasic dielectric systems, both of which contain BT in a polymeric host (i.e., similar dielectric contrast and volume fractions to those studied). It should be pointed out that the permittivity of BT powder is highly sensitive to the grain size<sup>24–28</sup> It has been reported that coarse-grained BT (20–50  $\mu\text{m}$ ) shows

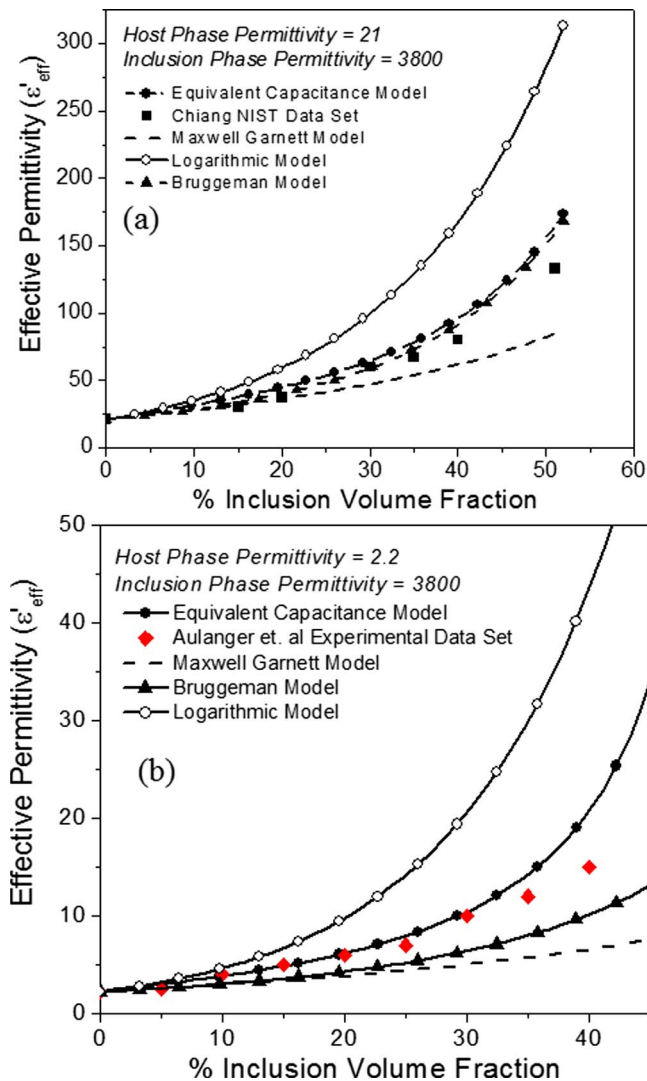


FIG. 9. (Color online) Effective permittivity of the diphasic composite as predicted by the equivalent capacitance model and its comparison to experimental data with host phase permittivities of 21 and 2.2.

$\epsilon_r=1500$ – $2000$  at room temperature, whereas the permittivity for fine-grained BT ( $\sim 1 \mu\text{m}$ ) is  $3500$ – $4000$ . As the grain size decreases below  $1 \mu\text{m}$ , the permittivity will most likely be around  $950$ – $1200$ .

The first system experimentally investigated by Chiang and Popielarz<sup>29</sup> contains cyanoresin as a host phase ( $\epsilon_h=21$ ) and BT with grain size less than  $2 \mu\text{m}$  as the inclusion phase. The exact data on inclusion permittivity have not been reported,<sup>29</sup> so the BT permittivity is assumed to be approximately  $\epsilon_i=3800$ , in accordance with the permittivity of BT with grain size less than  $2 \mu\text{m}$ . In this case, the dielectric contrast is 180. The volume fraction of the inclusion phase in the equivalent circuit model is varied between 0 and 52 vol %. Figure 9(a) shows the experimental effective permittivity as a function of the inclusion volume fraction for this system, as well as the dependencies calculated based on different models.

The second experimental system,<sup>30</sup> which the equivalent capacitance model is compared, contains polypropylene as a host phase ( $\epsilon_h=2.2$ ), and BT as an inclusion phase ( $\epsilon_i=3800$ ). In this case, the dielectric contrast is  $\sim 1700$ . Using

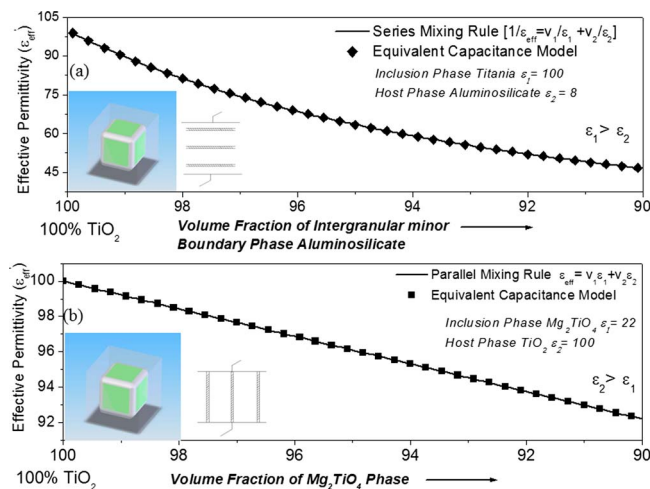


FIG. 10. (Color online) Comparison of effective permittivity predictions of series and parallel mixing rule with equivalent capacitance model.

these parameters, the effective permittivity as a function of the inclusion volume fraction is shown in Fig. 9(b).

The computations based on the equivalent capacitance model agree with the experimental data. The first set of experimental data for inclusion volume fraction less than 40% has the discrepancy of less than 15% [data of Ref. 29, seen in Fig. 9(a)]. As seen Fig. 9(b), for the 40% inclusion volume fraction the maximum discrepancy does not exceed 25%.

The equivalent capacitance model agrees satisfactorily with experimental data. The equivalent capacitance model also agrees well with the Bruggeman<sup>12</sup> predictions, especially for the first case of the lower dielectric contrast. The equivalent capacitance model provides a better fit to the experimental results than the MG and logarithmic mixing rules. The discrepancy between experimental data and the model prediction can arise from numerous factors. Some of the reasons are the following. The equivalent capacitance model has been developed for an ordered system, while the real-world composites have inclusions randomly dispersed in the host phase. Although the reported experimental systems are for 0–3 composites, the actual inclusion shape in these composites might not be exactly spherical.

An equivalent capacitance model has also been applied to model diphasic structures, in which the inclusion volume fraction is higher than that in the previously considered cases ( $V_f > 90\%$ ). The results of modeling using the equivalent capacitance model have been compared with the results of two known mixing rules: series and parallel mixing.<sup>1</sup> These two models were used by Payne<sup>1</sup> to study the effective permittivity of real-world composites, such as liquid phase sintered BT. The composites in these models are represented as layered structures, either series or parallel, depending on the ratio of permittivities of phases. If the inclusion phase has a significantly higher permittivity than the host (dielectric contrast  $\geq 10$ ), a series mixing rule may be used to predict the effective permittivity of the composite due to the local electric field behavior. If the inclusion phase has a lower permittivity than the host, a parallel mixing rule may be used.

Figure 10(a) shows a comparison of the predicted effective permittivity of a dielectric composite as a function of

inclusion volume fraction for the series mixing rule and equivalent capacitance model. The system modeled in this case is a diphasic mixture of titania ceramics ( $\epsilon_1 = 100$ ) containing intergranular boundary phase of aluminosilicate ( $\epsilon_2 = 8$ ). The second system considered is a diphasic mixture of  $\text{TiO}_2$  ( $\epsilon_1 = 100$ ) and  $\text{Mg}_2\text{TiO}_4$  ( $\epsilon_2 = 22$ ). This system is modeled using the parallel mixing rule, which is also compared to the equivalent capacitance model in Fig. 10(b). The predictions of the equivalent capacitance model match the series and parallel mixing rules for the appropriate composite structures.

The series and parallel mixing rules represent limiting cases of the more general equivalent capacitance model. This implies that the equivalent capacitance model may be used to describe effective permittivity of a wide range of diphasic dielectric microstructures.

To further validate the basic fundamental idea of equivalent capacitance model, predictions for effective permittivity have been tested based on the direction of discretization. It is found that effective permittivity predictions are independent of the direction of discretization (Appendix C). The equivalent capacitance model can also account for the inclusion orientation and high aspect ratio inclusions. A demonstrative example is shown in Appendix D.

In this publication, equivalent capacitance model is proposed for ordered composites. The similarities and differences between the macroscopic behavior of ordered and random composites are ongoing areas of research. It is imperative that future studies include simulations of random inclusion geometries. These studies could be achieved by consideration of a 3D array of cubes representing the host phase. By using probability theory, it is possible to allocate a particular probability of cells filled with inclusions as opposed to cells that are empty. Thus, a random composite could be analytically created and modeled. The equivalent capacitance/impedance model could then be applied for evaluating the effective properties of the composite and compared with ordered systems and real-world systems.

The study of dielectric composites has been, unfortunately, divided between theorists and experimentalists. There is a need for a unified approach toward examination of composite electrical properties. Many investigators continue to apply effective medium theories and other analytical models without being cognizant of the fact that the relevance of these models, fitted to one data set, may not be applicable to other material or microstructural systems. This issue is complicated by the fact that the permittivity of the inclusion particle is a function of particle size, and this is often not measured, or is unknown. This results in the use of permittivity values that best fit the results. Theorists on the other hand continue to compare their mixing rule approaches with other models and bounds and not with experimental results. A joint approach needs to be adopted that would look at the following issues:

- measurement of inclusion particle size distribution,
- measurement of slurry properties and, thereby, deduction of inclusion phase permittivity,
- impact of dispersant on composite polarization response,



particularly at the interface between the particle and host phase, and

- incorporation of these data into mixing models for both ordered and random systems to predict effective properties.

At this point, it is imperative to be able to objectively analyze the equivalent capacitance model and be able to identify its strengths and limitations. A key feature of this model is its independence of the inclusion size limitations associated with traditional mixing theories and the ability to uniformly apply this mixing theory to any composite dielectric architecture (0–3, 2–2, 1–3, and 3–3). The equivalent capacitance/impedance model developed has also been extended to complex geometries (*high aspect ratio inclusions*) and high volume fractions of high phase permittivity systems. The advantage of equivalent capacitance model is that it is a unique approach to take into account shape characteristics of the inclusion. It avoids reliance on approximating the shape to give approximate shape factors. This results in accurate accounting for the shape of inclusion. Although this aspect is its strength, it also necessitates developing algorithms for complex shapes. This would take this mixing method from realm of being an analytical tool toward numerical methods, which was not the intention of this research work from the outset.

It is also important to acknowledge that the equivalent capacitance model does not take into account interfacial polarization, and therefore, comparing model predictions with experimental results in which interfacial contributions are present might not be the best approach to validate the model. Hence, a dual approach of comparing model predictions with experimental data and also with other mixing theory has been adopted.

#### IV. CONCLUSIONS

An equivalent capacitance model to estimate the static effective permittivity of a composite mixture based on discretizing a dielectric body into partial capacitor elements was presented. The model was demonstrated for a system consisting of high-permittivity spherical inclusion(s) in a cube of a lower permittivity phase (e.g., a 0–3 composite), as well as for a periodic system of such individual cells. The predictions of the equivalent capacitance model agree well with experimental data obtained from the literature. The results of computations show that the classical MG and equivalent capacitance models diverge at inclusion volume fractions greater than approximately 10% since the MG model is valid for only dilute mixtures. The present model based on discretization of the dielectric volume has no inherent restrictions on inclusion volume fraction, size, or shape, and is applicable to any structure subjected to an applied homogeneous static electric field.

Effective permittivity predictions by the equivalent capacitance model match the limiting case series and parallel mixing rules. This implies that the equivalent capacitance model is applicable to a wide range of composite microstructures. Extension of the equivalent capacitance model to predict frequency-dispersive relative permittivity of composites

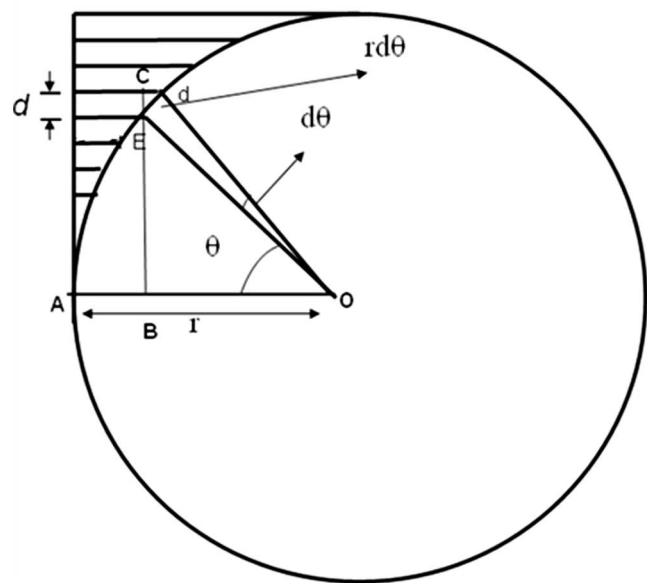
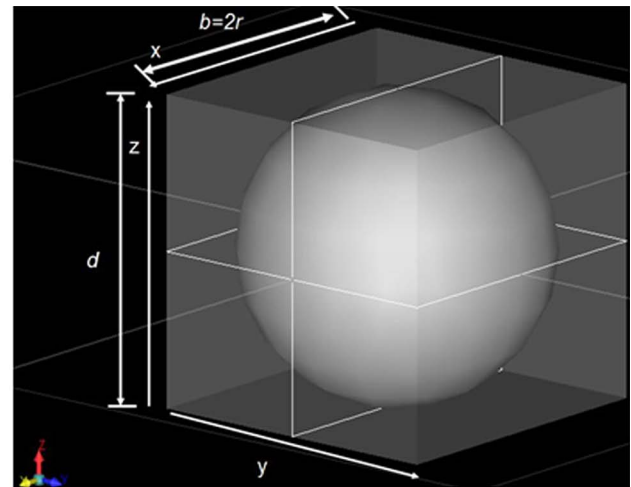


FIG. 11. (Color online) 3D views of the corner capacitor element and vertically cut section of inclusion sphere and corners detailing the discretization process for calculating the corner capacitance value.

has also been developed by including loss in the model, assigning partial resistances along with the partial capacitances (*RC* circuits). This extension of the model is described in a separate paper. The equivalent capacitance model may also be extended to the case of randomly dispersed inclusions.

#### ACKNOWLEDGMENTS

This work was supported through a MURI program sponsored by the Office of Naval Research under Grant No. N000-14-05-1-0541.

#### APPENDIX A: CALCULATION OF THE CORNER CAPACITANCE

Consider the corner capacitor elements, as shown in Fig. 11. Their dimensions are characterized by parameters  $b$  and  $d$ .  $b=2r$  is equal to the diameter of the sphere, as the cube dimension in which the inclusion sphere is enclosed.  $d$  is the thickness of the plates. The angle  $\theta$  is measured from the horizontal direction, and  $d\theta$  is an increment.

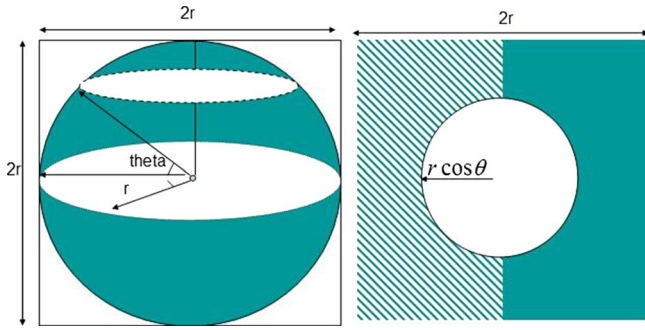


FIG. 12. (Color online) Sectional front and top views of the inclusion sphere and corner elements to explain mathematics of the discretization process.

The area of the corner capacitors can be calculated using 3D visualization, as illustrated in Figs. 11 and 12. The area of the discretized corner plate can be calculated from Fig. 12. Thus, an expression for the area of the discretized corner capacitor plate may be written as

$$S = 2r^2 - \frac{\pi r^2 \cos^2 \theta}{2}. \tag{A1}$$

From the triangle  $\Delta EDO$ , the length ED is

$$l(ED) = \sin(d\theta). \tag{A2}$$

As the angle  $d\theta$  is very small,

$$l(ED) \approx rd\theta. \tag{A3}$$

From the triangle  $\Delta ECD$ , the incremental thickness  $dh$  of any discretized plate can be found as

$$dh = l(EC) = r \cos \theta d\theta. \tag{A4}$$

The incremental capacitance of every corner plate is calculated as follows:

$$dC_i = \frac{\epsilon_0 \epsilon_h \left( 2r^2 - \frac{\pi r^2 \cos^2 \theta}{2} \right)}{r \cos \theta dh}. \tag{A5}$$

All the discretized corner capacitors are arranged in series and therefore the equivalent capacitance of the corner elements is given by the following expression:

$$\frac{1}{C_d} = \frac{1}{C_1} + \frac{1}{C_2} + \dots + \frac{1}{C_n} = \frac{1}{\sum_{i=1}^n \frac{1}{C_i}} = \frac{1}{\int_0^{\pi/2} \frac{1}{dC_i}}. \tag{A6}$$

Therefore, the corner capacitance is calculated by the expression shown in Eq. (A6),

$$C_d = \frac{1}{\int \frac{1}{dC_i}} = \frac{1}{2 \int_0^{\pi/2} \frac{d \sin \theta}{(4 - \pi)\epsilon_0 \epsilon_h r + \pi \epsilon_0 \epsilon_h r \sin^2 \theta}}. \tag{A7}$$

By substituting  $\sqrt{\pi \epsilon_0 \epsilon_h r} \sin \theta = X$  and  $A^2 = \epsilon_0 \epsilon_h r (4 - \pi) / \sqrt{\pi \epsilon_0 \epsilon_h r}$  results in the expression below,

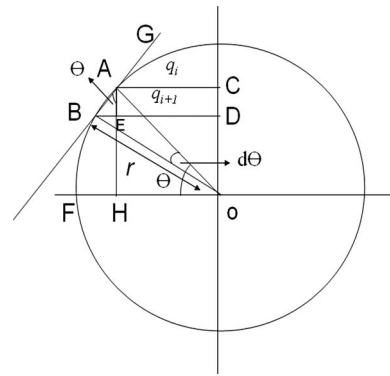


FIG. 13. Vertically cut section of inclusion sphere detailing the discretization process for calculating the capacitance value of inclusion dielectric sphere.

$$C_d = \frac{1}{2 \int_0^{\pi/2} \frac{dX}{A^2 + X^2}} = \frac{\epsilon_0 \epsilon_h r \pi}{2} \cdot \frac{1}{\frac{1}{\sqrt{\frac{4}{\pi} - 1}} \arctan \left[ \frac{1}{\sqrt{\frac{4}{\pi} - 1}} \right]}. \tag{A8}$$

**APPENDIX B: CALCULATION OF THE CAPACITANCE OF DIELECTRIC SPHERE**

A dielectric sphere inside a parallel-plate capacitor with voltage applied to its top and bottom plates is discretized by horizontal slices of the sphere, as shown in Fig. 13. Let us consider just a quarter of the sphere shown in Fig. 13.

The distance AC, which is the radius of the slice, is labeled as  $q_i$ , and the incremental distance is

$$\Delta q_i = q_{i+1} - q_i. \tag{B1}$$

Angle  $\angle AOF = \theta$ , and the increment of the angle  $\angle AOB = d\theta$ . From  $\Delta AOB$ , it is seen that

$$\sin d\theta = \frac{l(AB)}{l(AO)}. \tag{B2}$$

Since  $\angle AOB = d\theta$  is very small,

$$l(AB) = r \sin(d\theta) \approx rd\theta. \tag{B3}$$

$\angle AOF$  and  $\angle CAO$  are equal, as they are internal alternate angles, and

$$\angle CAO + \angle OAE = 90^\circ \Rightarrow \angle OAE = (90^\circ - \theta). \tag{B4}$$

Then,

$$\angle CAO + \angle EAB = 90^\circ. \tag{B5}$$

By substituting  $\angle OAE$  of Eq. (B4) into Eq. (B5), one can get

$$\angle EAB = \theta. \tag{B6}$$

From  $\Delta AEB$ , one can find the thickness of the individual discretized plate  $d$ ,

$$\cos \theta = \frac{l(AE)}{l(AB)}. \quad (B7)$$

Therefore, the thickness of the discretized capacitor is given by

$$d = r \cos \theta d\theta. \quad (B8)$$

Lengths OH and AC are

$$l(AC) = l(OH) = q_i. \quad (B9)$$

From the triangle  $\Delta OEH$ , it may be determined that

$$q_i = l(OH) = r \cos \theta. \quad (B10)$$

Only half area of the discretized plate is taken into account as the sphere is divided into four quarters. The area of the discretized capacitor plates is given by

$$\text{area} = \pi(r \cos \theta)^2. \quad (B11)$$

The capacitance of the discretized plates can be calculated as

$$C_i = \frac{\epsilon_0 \epsilon_i \pi (r \cos \theta)^2}{2R d \theta \cos \theta}. \quad (B12)$$

The inverse value is

$$\frac{1}{C_i} = \frac{2d\theta}{\epsilon_0 \epsilon_i \pi r \cos \theta}. \quad (B13)$$

The total capacitance of the quarter of the sphere is calculated as a series capacitance, so

$$\frac{1}{C_{1/4}} = \frac{2}{\pi r \epsilon_0 \epsilon_i} \int_0^{\pi/2} \frac{d\theta}{\cos \theta}. \quad (B14)$$

Finally,

$$C_{1/4} = \frac{\pi r \epsilon_0 \epsilon_i}{2 \int_0^{\pi/2} \frac{d\theta}{\cos \theta}}. \quad (B15)$$

This capacitance  $C_{1/4}$  is the capacitance of the quarter of the sphere, but it is also a total capacitance of the whole dielectric sphere since two left hand capacitances are in series, two right-hand capacitances are also in series, and they are connected together in parallel,

$$C_5 = C_{1/4}. \quad (B16)$$

### APPENDIX C: DIRECTION OF DISCRETIZATION

The equivalent capacitance model relies on its ability to discretize a diphasic composite body to predict the effective properties of composite. In order to validate the equivalent capacitance model, demonstrating that the model predictions are independent of the direction of the discretization is required. Two discretization pathways were identified to test the equivalent capacitance model. The first strategy is a horizontal discretization pathway and the second is a vertical discretization approach. Two-dimensional views of these discretization schemes are presented in Fig. 14. As anticipated based on physical principles, it was found that the predictions of effective permittivity for both cases of horizontal as well vertical discretizations were similar. However, the inte-

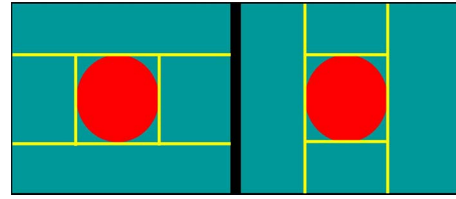


FIG. 14. (Color online) Horizontal and vertical schemes of discretizations.

gration schemes employed for the calculation of the corner capacitances lead to minor discrepancies at low inclusion volume fractions.

The effective permittivity predictions for a system of host phase permittivity of 4 and an inclusion phase permittivity of 1900 as a function of inclusion volume fraction are shown in Fig. 15. The primary condition that needs to be satisfied for predictions of the equivalent capacitance model to be independent of the discretization approach is that the permittivity of each phase is isotropic, as illustrated in the following equation:

$$\epsilon(x, y, z) = \epsilon_x(x) \cdot \epsilon_y(y) \cdot \epsilon_z(z). \quad (C1)$$

### APPENDIX D: ORIENTATION DEPENDENCE OF PERMITTIVITY

Many experimental studies have been done regarding the impact of high aspect ratio of inclusions on the effective permittivity.<sup>31</sup> It is also important to verify that the equivalent capacitance model can account for orientation dependence, as for the case of 1–3 composites. An inclusion with an aspect ratio of 3:1 was assumed to be present in the host phase oriented in the vertical direction, and then the inclusion orientation was in the horizontal direction. An enhancement in permittivity is expected for the vertically oriented inclusion or for the case of spherical inclusions that are aligned with the applied electric field, as illustrated in Fig. 16. This figure, which presents predictions of the equivalent circuit model, illustrates that the model can capture particle

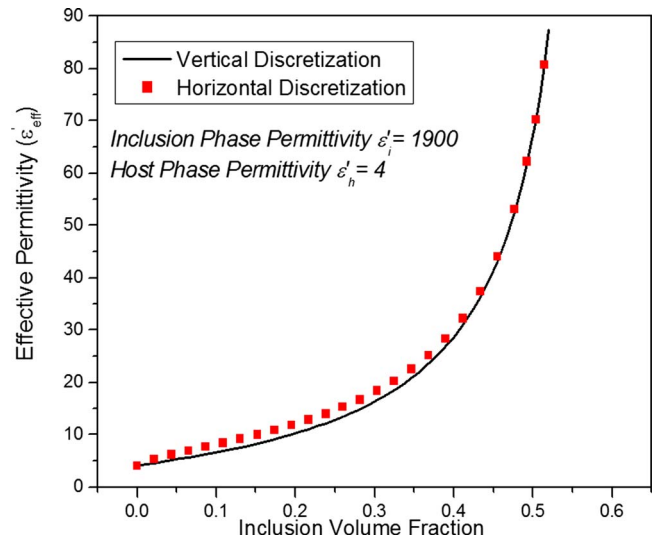


FIG. 15. (Color online) Equivalent capacitance model predictions for effective permittivity as a function of inclusion volume fraction for both horizontal and vertical discretization approaches.

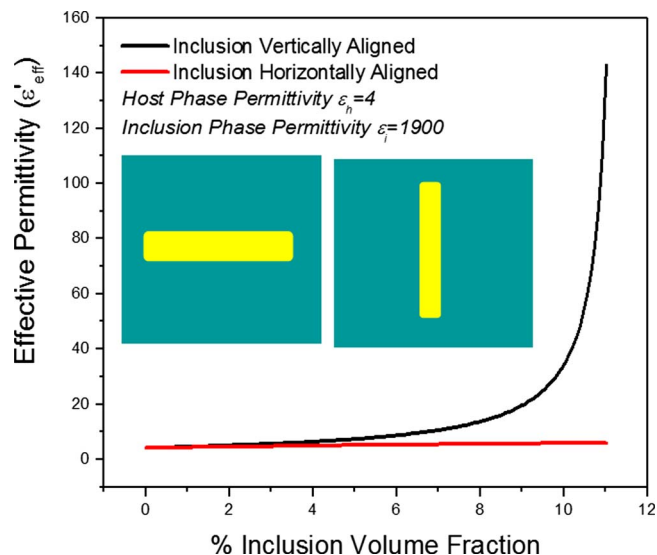


FIG. 16. (Color online) Equivalent capacitance model predictions for effective permittivity as a function of inclusion orientation.

orientation effects. This capability of the model illustrates one of the benefits of the equivalent capacitance approach that has been developed compared to simple mixing rule methods. These methods are typically limited to predictions of volume fraction effects and are incapable of predicting particle orientation effects.

<sup>1</sup>S. D. Poisson, *Mem. Acad. R. Sci. Inst.* **5**, 247 (1821); see also L. K. H. Ven Beck, *Prog. Dielectr.* **7**, 71 (1967); see also D. A. Payne, Ph.D. thesis, The Pennsylvania State University, 1973.

<sup>2</sup>L. Rayleigh, *Philos. Mag.* **44**, 28 (1897); see also T. C. Choy, *Effective Medium Theory, Principles and Applications* (Oxford University Press, Oxford, 1999).

<sup>3</sup>J. C. M. Garnett, *Philos. Trans. R. Soc. London, Ser. B* **203**, 385 (1904); see also H. Frohlich, *Theory of Dielectrics*, 2nd ed. (Oxford University, London, 1958); see also P. S. Neelakanta, *Handbook of Electromagnetic Materials* (CRC, Boca Raton, FL, 1995).

<sup>4</sup>R. Landauer, in *Electrical Transport and Optical Properties of Inhomogeneous Media*, AIP Conference Proceedings No. 40, edited by J. C. Garland and D. B. Tanner (American Institute of Physics, New York, 1978).

<sup>5</sup>D. J. Bergman and D. Stroud, in *Solid State Physics*, edited by H. Ehrenreich and D. Turnbull (Academic, New York, 1992), Vol. 46, pp. 178–320.

<sup>6</sup>A. Sihvola, *Electromagnetic Mixing Formulas and Applications* (IEE, London, UK, 1999).

<sup>7</sup>M. Y. Koledintseva, J. Wu, J. Zhang, J. L. Drewniak, and K. N. Rozanov, *Proceedings of IEEE Symposium on Electromagnetic Compatibility Vol. 1*, Santa Clara, CA, 2004, pp. 309–314.

<sup>8</sup>J. Avelin and A. Sihvola, *Microwave Opt. Technol. Lett.* **32**, 60 (2002).

<sup>9</sup>O. Weiner, *Nachr. Ges. Wiss. Goettingen, Math.-Phys. Kl.* **32**, 509 (1912); see also D. A. Payne, Ph.D. thesis, The Pennsylvania University, 1973.

<sup>10</sup>D. F. Rushman and M. A. Striven, *Proc. Phys. Soc. London* **59**, 1011 (1947).

<sup>11</sup>W. D. Kingery, *Introduction to Ceramics* (Wiley, New York, 1960).

<sup>12</sup>D. A. G. Bruggeman, *Ann. Phys.* **24**, 636 (1935); see also B. Sareni, L. Krahenbuhl, A. Beroual, and C. Brosseau, *J. Appl. Phys.* **83**, 3288 (1998).

<sup>13</sup>V. Myroshnychenko and C. Brosseau, *J. Appl. Phys.* **97**, 044101 (2005).

<sup>14</sup>K. Lichtenecker, *Phys. Z.* **10**, 1005 (1909); see also P. S. Neelakanta, *Handbook of Electromagnetic Materials* (CRC, Boca Raton, FL, 1995).

<sup>15</sup>D. Payne, *Tailoring Multiphase and Composite Ceramics, Material Science Research*, edited by R. E. Tressler, G. L. Messing, and C. G. Pantano (Plenum, New York, 1987), Vol. 20, pp. 413–431.

<sup>16</sup>C. J. Dias and D. K. Das-Gupta, *IEEE Trans. Dielectr. Electr. Insul.* **3**, 706 (1996).

<sup>17</sup>C. J. Dias and D. K. Das-Gupta, *Key Eng. Mater.* **92**, 217 (1994).

<sup>18</sup>Y. Bai, Z. Y. Cheng, V. Bharti, H. S. Xu, and Q. M. Zhang, *Appl. Phys. Lett.* **76**, 3804 (2000).

<sup>19</sup>Y. Rao, S. Ogitan, P. Kohl, and C. P. Wong, *J. Appl. Polym. Sci.* **83**, 1084 (2002).

<sup>20</sup>C. Huang and Q. M. Zhang, *Adv. Funct. Mater.* **14**, 501 (2004).

<sup>21</sup>Y. Rao, S. Ogitan, P. Kohl, and C. P. Wong, *Electronic Components and Technology Conference, 2000* (unpublished), pp. 183–187.

<sup>22</sup>B. Chu, X. Zhou, K. Ren, B. Neese, M. Lin, Q. Wang, F. Bauer, and Q. M. Zhang, *Science* **313**, 334 (2006).

<sup>23</sup>S. V. Marshall, R. E. Du Broff, and G. G. Skitek, *Electromagnetic Concepts and Applications*, 4th ed. (Prentice-Hall, Englewood Cliffs, NJ, 1996).

<sup>24</sup>G. Arlt, D. Henning, and G. de With, *J. Appl. Phys.* **58**, 1619 (1985).

<sup>25</sup>G. Arlt, *J. Mater. Res.* **25**, 2655 (1990).

<sup>26</sup>G. Arlt, *Ferroelectrics* **104**, 217 (1990).

<sup>27</sup>K. Uchino, E. Sadanaga, and T. Hirose, *J. Am. Ceram. Soc.* **72**, 1555 (1989).

<sup>28</sup>R. Waser, *Ferroelectrics* **15**, 39 (1997).

<sup>29</sup>C. Chiang and R. Popielarz, *Ferroelectrics* **275**, 1 (2002).

<sup>30</sup>E. Aulagner, J. Guilet, G. Seytre, C. Hantouche, P. Le Gonidec, and G. Tezulli, *Proceedings of the IEEE Fifth International Conference on Conduction and Breakdown in Solid Dielectrics*, Leicester, UK (IEEE, Piscataway, NJ, 1995), p. 423.

<sup>31</sup>C. P. Bowen and R. E. Newnham, *J. Mater. Res.* **13**, 205 (1998).